

# Physical origin of the buckling in CuO<sub>2</sub>: Electron-phonon coupling and Raman spectra

M. Opel and R. Hackl

Walther Meissner Institut für Tieftemperaturforschung, Garching, D-85748, Germany

T. P. Devereaux

Department of Physics, The George Washington University, Washington, DC 20052

A. Virosztek and A. Zawadowski

Institute of Physics and Research Group of the Hungarian Academy of Sciences, Technical University of Budapest, H-1521  
Budapest, Hungary

and Research Institute for Solid State Physics, P.O.Box 49, H-1525 Budapest, Hungary

A. Erb and E. Walker

DPMC, Université de Genève, CH-1211 Genève, Switzerland

H. Berger and L. Forró

EPFL, Ecublens, CH-1015 Lausanne, Switzerland

(June 21, 2021)

It is shown theoretically that the buckling of the CuO<sub>2</sub> planes in certain cuprate systems can be explained in terms of an electric field across the planes which originates from different valences of atoms above and below the plane. This field results also in a strong coupling of the Raman-active out-of-phase vibration of the oxygen atoms ( $B_{1g}$  mode) to the electronic charge transfer between the two oxygens in the CuO<sub>2</sub> plane. Consequently, the electric field can be deduced from the Fano-type line shape of the  $B_{1g}$  phonon. Using the electric field estimated from the electron-phonon coupling the amplitude of the buckling is calculated and found to be in good agreement with the structural data. Direct experimental support for the idea proposed is obtained in studies of YBa<sub>2</sub>Cu<sub>3</sub>O<sub>6+x</sub> and Bi<sub>2</sub>Sr<sub>2</sub>(Ca<sub>1-x</sub>Y<sub>x</sub>)Cu<sub>2</sub>O<sub>8</sub> with different oxygen and yttrium doping, respectively, including antiferromagnetic samples. In the latter compound, symmetry breaking by replacing Ca partially by Y leads to an enhancement of the electron-phonon coupling by an order of magnitude.

PACS numbers: 74.72.-h, 63.20.Kr, 78.20.Bh, 71.10.-w

## I. INTRODUCTION

The physical origin of the buckling of the CuO<sub>2</sub> plane in certain high temperature superconductors, where the oxygen atoms are placed outside of the plane of the copper atoms, is a long standing problem. There are two possible explanations: (i) the surroundings of the CuO<sub>2</sub> plane is not symmetrical, thus an electric field perpendicular to the plane acting on atoms with different charges deforms that plane, and (ii) the energy associated with chemical bonds (especially the bond between the oxygen  $\pi$ -orbitals perpendicular to the plane and the coppers) results in a spontaneous symmetry breaking. The present paper provides direct experimental evidence to support the first possibility in accordance with the theory.

It has been suggested previously [1] that in the presence of a perpendicular electric field a charge transfer between the two different oxygens O(2) and O(3) invokes a deformation of the type of the  $B_{1g}$  Raman-active phonon at 330cm<sup>-1</sup>, where the two oxygens move in an out of phase manner perpendicular to the plane (Fig. 1a). The resulting electron-phonon coupling was then used to interpret the Fano interference in the Raman spectra of YBa<sub>2</sub>Cu<sub>3</sub>O<sub>6+x</sub> (Y-123), where the light is scattered by both the  $B_{1g}$  phonon and the electrons involved in the charge transfer in the plane described above. For a CuO<sub>2</sub> plane in a more symmetrical environment (where the electric field is negligible) such a linear coupling does not exist since the energy correction due to the deformation of the chemical bonds is at least quadratic in the displacement of the oxygens. Hence, only much weaker two-phonon processes contribute.

The coupling strength and, consequently, the value of the electric field perpendicular to the plane can be determined from the Fano line shape of the  $B_{1g}$  phonon using the expressions derived in Ref. [1]. In order to follow closely the doping dependence of the line shape we will use here, in contrast to [1], a more realistic three band model for the electronic system. It will be described in some detail thus augmenting an earlier publication which gave just a brief summary [2]. The Raman- active continuum which interferes with the  $B_{1g}$  phonon is assumed to originate from strongly relaxing electrons in a single conduction band such as proposed in Refs. [3–5] and will be introduced

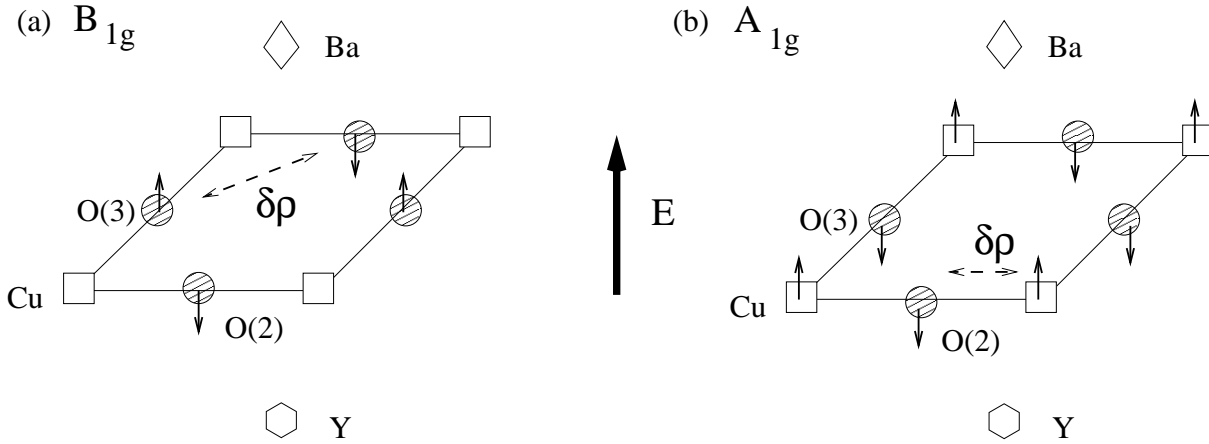


FIG. 1. The unit cell of the  $\text{CuO}_2$  plane in Y-123 shown with the atomic displacements corresponding to the  $B_{1g}$  (a) and  $A_{1g}$  (b) phonons. The electric field  $E$  perpendicular to the planes is due to the asymmetric environment ( $\text{Ba}^{2+}$  above,  $\text{Y}^{3+}$  below), and causes a static deformation of the  $A_{1g}$  type, usually referred to as buckling (also called dimpling as in Ref. [11]).  $\delta\rho$  and the double arrows denote the charge transfer which accompanies the lattice vibration. In Bi-2212,  $\text{Ba}^{2+}$  is replaced by  $\text{Sr}^{2+}$  and, at optimal doping,  $\text{Y}^{3+}$  by  $\text{Ca}^{2+}$ . Then the electrical field  $E$  is negligible.

phenomenologically as in [1]. Recently, Sherman and coworkers considered the coupling of the  $B_{1g}$  phonon to non-interacting Bloch electrons including intra and inter-band intermediate states in order to understand the phonon intensity [6]. Here, the focus is placed on the interference of the phonon and the electronic continuum which are excited by the light through two initially independent channels. In our approach the direct coupling of the phonon to the light is parameterized and not explicitly considered. Our goal is to better understand the interaction between the phonon and the conduction electrons. Therefore, both Y-123, where the surroundings of the  $\text{CuO}_2$  plane is highly asymmetric, and  $\text{Bi}_2\text{Sr}_2\text{CaCu}_2\text{O}_8$  (Bi-2212), where the plane is placed in a more symmetrical position with respect to the charges of the nearby atoms, will be studied.

The  $B_{1g}$  phonon in metallic cuprate systems has actually been studied intensively by several groups [2,7–9]. The main emphasis was placed on the anomalies at the transition to the superconducting state. It was shown, for instance, that the change in frequency of the  $B_{1g}$  phonon at  $T_c$  vanishes already at moderate underdoping [9] pointing at a considerable change in the electron-phonon coupling. While the phonon renormalization at  $T_c$  has been the subject of numerous theoretical treatments [10], no attempt has been made yet to link the doping dependence of the coupling to a realistic band structure, i.e. a microscopic model. For a comparison with the model predictions, a systematic experimental study of the phonon covering the complete doping range from antiferromagnetic (AF) insulating to slightly overdoping in comparable, high-quality samples is essential. Therefore, we present not only data on differently doped metallic samples but also new data on undoped antiferromagnetic ones in order to get an idea of the intrinsic line width and to study in detail the influence of a reduction of the continuum scattering on the line shape of the phonon.

As already shown earlier [2,7] the  $B_{1g}$  phonon has a reasonably Lorentzian line shape for the symmetric compound Bi-2212 indicating the lack of any substantial coupling between that phonon and the charge transfer between the two oxygens in accordance with the absence of an electric field. This striking difference to the data of Y-123 [8] can be considered as strong evidence in favor of the linear (involving one phonon) electron-phonon coupling due to the electric field. In order to complete this argument, we gradually replace  $\text{Ca}^{2+}$  by  $\text{Y}^{3+}$  in the Bi-2212 compound where the doping most likely breaks locally the approximate reflection symmetry through the  $\text{CuO}_2$  plane, thereby making this material similar to Y-123. In fact, the phonon becomes more asymmetric and the electron-phonon coupling increases by an order of magnitude [2]. However, this increase does not at all result in an enhancement of the superconducting transition temperature:  $T_c$  is rather reduced on substituting Ca with Y and follows the usual  $T_c$  vs. doping curve.

Finally, the value for the electron-phonon coupling obtained from the analysis of the line shape is found to be in excellent agreement with the value calculated from the magnitude of the electric field due to the experimentally observed buckling [12] and the restoring force calculated from the frequency of the  $A_{1g}$  phonon (Fig. 1b). The coupling depends on changes in the doping via the proximity of the van Hove singularity in the density of states to the Fermi level  $E_F$ .

The paper is organized as follows: In section II the theoretical model is described in some detail and the relevant expressions are derived. In section III and IV experimental details and results are being given. Finally, the consequences are discussed.

## II. THEORETICAL MODEL

Much of the development of the crystal field model was given in Ref. [1], and details of the calculations are found therein. We start with this and only point out where changes are made. The model constructed in Ref. [1] started from a three band model where only the Cu-O hopping was taken into consideration. However, one must add O-O hopping in order to represent the curvature and centering of the Fermi surface as revealed from angle-resolved photo-emission experiments. Therefore we augment the results from [1] to include direct O-O hopping. We start by first considering a simple 3 band model for the CuO<sub>2</sub> plane with Cu-O hopping amplitude  $t$  and O-O hopping amplitude  $t'$ :

$$H_0 = \varepsilon \sum_{\mathbf{n},\sigma} b_{\mathbf{n},\sigma}^\dagger b_{\mathbf{n},\sigma} + t \sum_{\mathbf{n},\sigma,\delta} [P_{\delta} b_{\mathbf{n},\sigma}^\dagger a_{\mathbf{n},\sigma,\delta} + h.c.] + t' \sum_{\mathbf{n},\sigma} \sum_{\langle \delta, \delta' \rangle} P'_{\delta,\delta'} a_{\mathbf{n},\delta,\sigma}^\dagger a_{\mathbf{n},\delta',\sigma}, \quad (1)$$

where  $b_{\mathbf{n},\sigma}^\dagger$  creates an electron with spin  $\sigma$  at a copper lattice site  $\mathbf{n}$ , while  $a_{\mathbf{n},\sigma,\delta}$  annihilates an electron at one of the neighboring oxygen sites  $\mathbf{n} + \delta/2$  determined by the unit vector  $\delta$  assuming the four values,  $(\pm 1, 0)$  and  $(0, \pm 1)$ . An oxygen atom between the two copper atoms at sites  $\mathbf{n}$  and  $\mathbf{n} + \delta$  is labeled by either  $(\mathbf{n}, \delta)$  or  $(\mathbf{n} + \delta, -\delta)$ . As in [1],  $\varepsilon = E_d - E_p$  is the difference of the Cu and O site energies and  $P_{\delta} = \pm 1$  depending on whether the orbitals (with real wavefunctions) have the same or opposite sign at the overlap region. Assuming Cu  $d_{x^2-y^2}$  and O  $p$  orbitals  $P_{-\delta} = -P_{\delta}$ , and we can choose  $P_{(1,0)} = 1$  and  $P_{(0,1)} = -1$ . Lastly,  $P'_{\delta,\delta'}$  denotes the overlap sign between an oxygen orbital at site  $\mathbf{n} + \delta/2$  with a neighboring oxygen orbital at site  $\mathbf{n} + \delta'/2$ . By our above convention these overlaps take the values  $P'_{\mathbf{x},\mathbf{y}} = P'_{-\mathbf{x},-\mathbf{y}} = 1$ ,  $P'_{\mathbf{x},-\mathbf{y}} = P'_{-\mathbf{x},\mathbf{y}} = -1$ , respectively. After Fourier transforming, the Hamiltonian now reads  $H^0 = \sum_{\mathbf{k},\sigma} H_{\mathbf{k},\sigma}^0$ , where

$$H_{\mathbf{k},\sigma}^0 = \varepsilon b_{\mathbf{k},\sigma}^\dagger b_{\mathbf{k},\sigma} + \{i b_{\mathbf{k},\sigma}^\dagger [a_{x,\mathbf{k},\sigma} t_x(\mathbf{k}) - a_{y,\mathbf{k},\sigma} t_y(\mathbf{k})] + h.c.\} + t'_\mathbf{k} [a_{x,\mathbf{k},\sigma}^\dagger a_{y,\mathbf{k},\sigma} + h.c.], \quad (2)$$

with the prefactors

$$t_\alpha(\mathbf{k}) = 2t \sin(ak_\alpha/2), \quad t'(\mathbf{k}) = -4t' \sin(ak_x/2) \sin(ak_y/2). \quad (3)$$

We can then easily diagonalize Eq. (2) and obtain the 3 bands:

$$H_{\mathbf{k},\sigma}^0 = \sum_{\beta} E_{\beta}(\mathbf{k}) d_{\beta,\mathbf{k},\sigma}^\dagger d_{\beta,\mathbf{k},\sigma}, \quad (4)$$

where  $\beta$  assumes the values  $+$ ,  $-$ , and  $0$  for the anti-bonding, bonding, and non-bonding bands, respectively. The energies are then given by solving a third order root equation and are

$$\begin{aligned} E_+(\mathbf{k}) &= s_+(\mathbf{k}) + s_-(\mathbf{k}) + \varepsilon/3 \\ E_-(\mathbf{k}) &= -\frac{1}{2}[s_+(\mathbf{k}) + s_-(\mathbf{k})] + \varepsilon/3 + \frac{i\sqrt{3}}{2}[s_+(\mathbf{k}) - s_-(\mathbf{k})] \\ E_0(\mathbf{k}) &= -\frac{1}{2}[s_+(\mathbf{k}) + s_-(\mathbf{k})] + \varepsilon/3 - \frac{i\sqrt{3}}{2}[s_+(\mathbf{k}) - s_-(\mathbf{k})] \end{aligned} \quad (5)$$

with

$$\begin{aligned} s_{\pm}(\mathbf{k}) &= (r(\mathbf{k}) \pm \sqrt{q^3(\mathbf{k}) + r^2(\mathbf{k})})^{\frac{1}{3}} \\ q(\mathbf{k}) &= -\frac{1}{3}[t_x^2(\mathbf{k}) + t_y^2(\mathbf{k}) + t'^2(\mathbf{k})] - \varepsilon^2/9 \\ r(\mathbf{k}) &= \frac{\varepsilon}{6}[t_x^2(\mathbf{k}) + t_y^2(\mathbf{k}) - 2t'^2(\mathbf{k})] - t'(\mathbf{k})t_x(\mathbf{k})t_y(\mathbf{k}) + \varepsilon^3/27 \end{aligned} \quad (6)$$

Since  $q^3(\mathbf{k}) + r^2(\mathbf{k})$  is negative for all  $\mathbf{k}$ ,  $s_+^*(\mathbf{k}) = s_-(\mathbf{k})$  and the energies are of course real.

The parameter values used,  $\varepsilon = 1\text{eV}$ ,  $t = 1.6\text{eV}$ , and  $t'/t = 0.35$ , are similar to those used in Ref. [11]. The dispersion for the three bands is plotted for symmetry  $\mathbf{k}$  points along the Brillouin zone (BZ) in Fig. 2 using these parameters and choosing the chemical potential such that the filling  $\langle n \rangle = 0.85$  for both spins. The upper (middle, lower) curve represents the band dispersion for the anti-bonding (non-bonding, bonding) band, respectively. Setting the direct O-O hopping integral  $t' = 0$  would yield a dispersionless non-bonding band whose energy equaled the oxygen site energy, while the other bands recover the dispersion calculated in Ref. [1]. The inset of Fig. 2 shows the

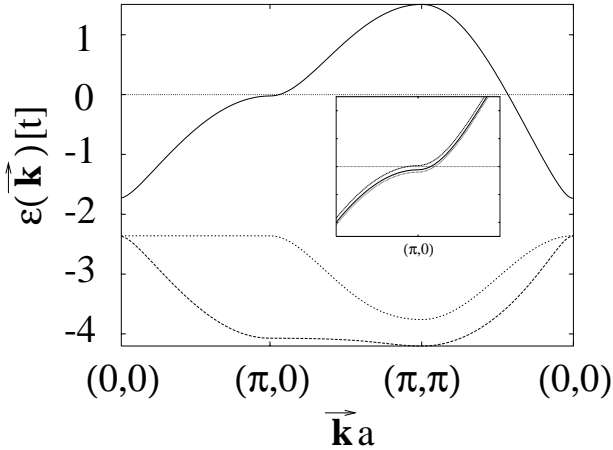


FIG. 2. Band dispersion for the 3-band model with nearest and next - nearest - neighbor hopping for the parameters listed in the text corresponding to optimally doped  $\text{YBa}_2\text{Cu}_3\text{O}_7$ . The upper (middle, lower) curve corresponds to the anti-bonding (non-bonding, bonding) band, respectively. Inset shows the doping dependence for the upper band only in the vicinity of the van Hove point near  $(\pi, 0)$ . The upper (middle, lower) curve represents over-(optimally, under-)doped systems, respectively.

dispersion of the anti-bonding band in the vicinity of the  $(\pi, 0)$  point in the BZ evaluated for different fillings which we label as over-doped ( $\langle n \rangle = 0.8$ ), optimally-doped ( $\langle n \rangle = 0.85$ ), and under-doped ( $\langle n \rangle = 0.875$ ), corresponding to the upper, middle, and lower curves in the inset, respectively. The filling changes the distance the flat part of the dispersion (van Hove point) is away from the Fermi level  $E_F$ , thus changing the density of states at  $E_F$ . Through this change in the density of states we attempt to understand the doping dependence of the coupling between the  $B_{1g}$  optical phonon mode and the conduction electrons.

At this point we can carry over the results from Ref. [1] with little loss of generality. As in Ref. [1] we consider only a reduced one band model appropriate for near half filling and take only the upper band  $E_+(\mathbf{k})$  into account. The electron - phonon reduced Hamiltonian for the  $B_{1g}$   $\mathbf{q} = 0$  phonon mode was given as

$$H_{el-ph} = \frac{1}{\sqrt{N}} \sum_{\mathbf{k},\sigma} g(\mathbf{k}) d_{\mathbf{k},\sigma}^\dagger d_{\mathbf{k},\sigma} [c + c^\dagger], \quad (7)$$

where  $N$  is the number of sites,  $d_{\mathbf{k},\sigma}$  annihilates an electron of spin  $\sigma$  and momentum  $\mathbf{k}$ , and  $c^\dagger$  creates a  $B_{1g}$  phonon mode of wavevector  $\mathbf{q} = 0$ . The coupling constant  $g(\mathbf{k})$  of the  $B_{1g}$  mode to an electron with momentum  $\mathbf{k}$  was evaluated in Ref. [1] and is given by

$$g(\mathbf{k}) = eE \sqrt{\frac{\hbar}{2M\omega_{B_{1g}}}} \frac{1}{\sqrt{2}} [|\phi_x(\mathbf{k})|^2 - |\phi_y(\mathbf{k})|^2], \quad (8)$$

where  $M$  is the oxygen mass,  $\omega_{B_{1g}}$  is the phonon frequency, and  $E$  is the  $\hat{\mathbf{z}}$ - component of the electric crystal field which for simplicity we take to be equal at both the O(2) and O(3) sites. The functions  $\phi_{x,y}$  are the amplitudes of the oxygen wave functions in the tight-binding wave functions of the upper band which arise from diagonalizing the three band model. In the absence of O-O hopping, these functions were given in [1]. Here, O-O hopping is included yielding

$$\begin{aligned} \phi_x(\mathbf{k}) &= \frac{-i}{N(\mathbf{k})} [E_+(\mathbf{k})t_x(\mathbf{k}) - t'(\mathbf{k})t_y(\mathbf{k})], \\ \phi_y(\mathbf{k}) &= \frac{i}{N(\mathbf{k})} [E_+(\mathbf{k})t_y(\mathbf{k}) - t'(\mathbf{k})t_x(\mathbf{k})], \\ \text{with } N^2(\mathbf{k}) &= [E_+^2(\mathbf{k}) - t'^2(\mathbf{k})]^2 + [E_+(\mathbf{k})t_x(\mathbf{k}) - t_y(\mathbf{k})t'(\mathbf{k})]^2 + [E_+(\mathbf{k})t_y(\mathbf{k}) - t_x(\mathbf{k})t'(\mathbf{k})]^2. \end{aligned} \quad (9)$$

We now are in a position to calculate the full Raman response. Again we can utilize the results derived in Ref. [1]. The generalized form of the Breit-Wigner or Fano lineshape describes the scattering of the light by the coupled electron-phonon system. The (independent) coupling strengths of the light to the phonon and to the electronic continuum with symmetry  $\lambda$  will be denoted by  $g_{p-p,\lambda}$  and  $\gamma_\lambda$ , respectively. The bare phonon when decoupled from

the conduction electrons is characterized by the energy  $\omega_\lambda$  and the intrinsic damping due to e.g. anharmonic phonon-phonon interaction by  $\Gamma_\lambda^i$ . The electronic continuum in symmetry channel  $\lambda$  will be described by the electronic susceptibility  $\chi_\lambda$ . It is clear that it cannot originate from a non interacting gas formed by Bloch electrons; it rather should be traced back to strong renormalization effects such as electron-electron interaction [3], spin-fermion [5] or to scattering on static impurities [4]. A parameterized form for  $\chi_\lambda$  is used which has been derived by one of us when electron dynamics is considered in materials with nesting properties along the Fermi surface [3]:

$$\chi_\lambda''(\omega) = N_F \frac{\omega \bar{\tau}_\lambda^{-1}}{\bar{\omega}^2 + \bar{\tau}_\lambda^{-2}}, \quad (10)$$

where

$$\begin{aligned} \bar{\tau}_\lambda^{-1} &= \tau_\lambda^{*-1} + \alpha \sqrt{(\beta' T)^2 + \omega^2}, \\ \bar{\omega} &= \omega m^*(\omega)/m, \\ \text{with } m^*(\omega)/m &= 1 + \frac{2\alpha}{\pi} \ln \left[ \frac{\omega_c}{\sqrt{(\beta' T)^2 + \omega^2}} \right]. \end{aligned} \quad (11)$$

Here  $N_F$  is the density of states for both spins at the Fermi level,  $m, m^*$  is the bare, renormalized electron mass, respectively,  $1/\tau_\lambda^* = 1/\tau - 1/\tau_\lambda$  is the channel-dependent impurity scattering rate reduced by vertex corrections [4] and  $\tau$  is the lifetime of the electrons.  $\alpha, \beta'$  and  $\omega_c$  are constants determined by a fit to the electronic continuum. The cut-off  $\omega_c$  is essentially the band width,  $\beta'$  measures the interaction between the electrons and can vary only between 3.3 and 4.2. They both will be fixed as indicated in Table I.  $\alpha \leq 1$  as long as  $\beta' \leq 3.7$  [3]. In addition,  $\alpha \cdot \beta'$  determines the temperature dependence of the normal-state d.c. resistivity and should therefore be close to 1.5. This means that there exist strong theoretical constraints for metallic samples.  $1/\tau_\lambda^*$  is a free parameter to get an optimal representation of the continuum. This form for the Raman susceptibility provides an adequate description to the continuum in the normal state of both Y-123 and Bi-2212 (see Ref. [3]). As the continuum depends only weakly on frequency it turns out that the choice of the parameters mildly influences the Fano line shape. The full Raman response measured in channel  $\lambda$  for the interacting electron-phonon system reads [1]:

$$\begin{aligned} \chi_{\lambda,full}''(\omega) &= \frac{(\omega + \omega_a)^2}{(\omega^2 - \hat{\omega}_\lambda^2)^2 + [2\omega_\lambda \Gamma_\lambda(\omega)]^2} \left\{ \gamma_\lambda^2 \chi_\lambda''(\omega) \left[ (\omega - \omega_a)^2 + 4\Gamma_\lambda^i \Gamma_\lambda(\omega) \left( \frac{\omega_\lambda}{\omega + \omega_a} \right)^2 \right] \right. \\ &\quad \left. + 4g_{p-p,\lambda}^2 \Gamma_\lambda^i \left( \frac{\omega_\lambda}{\omega + \omega_a} \right)^2 [1 + \lambda(\omega)/\beta]^2 \right\}. \end{aligned} \quad (12)$$

Here, the first factor on the right hand side is the Lorentzian line shape of the phonon modified by the Fano interference and the second one describes the interplay between the scattering of light on phonons and electrons. The details depend on the relation between the coupling constants  $g_{p-p,\lambda}$ , which has been studied by Sherman and coworkers [6],  $\gamma_\lambda$ , and  $\lambda_\lambda$ . The latter one describes the interaction of the phonon with the conduction electrons and can also be calculated directly from the band structure and the electric field by averaging the coupling  $g(\mathbf{k})$  given in Eq. (8) over the Fermi surface. For  $B_{1g}$  symmetry we obtain

$$g_{B_{1g}}^2 = -\frac{2}{N} \sum_{\mathbf{k}} |g(\mathbf{k})|^2 \frac{\partial f(\epsilon(\mathbf{k}))}{\partial \epsilon(\mathbf{k})}, \quad (13)$$

where  $f$  is the Fermi function and the factor of two accounts for both spin directions [13]. For convenience the dimensionless quantities  $\lambda(\omega)$  and  $\beta$  were introduced in Eq. (12) which depend on the coupling constants as follows

$$\lambda(\omega_{B_{1g}}) = \frac{2g_{B_{1g}}^2}{\omega_{B_{1g}}} \quad (14)$$

and

$$\beta = \frac{2g_{p-p,B_{1g}} g_{B_{1g}}}{\gamma_{B_{1g}} \omega_{B_{1g}} \sqrt{N_F}}. \quad (15)$$

$\lambda(\omega_{B_{1g}})$  is the usual electron-phonon coupling constant. Here the explicit dependence of  $\lambda(\omega)$  on  $\omega$  through  $\chi'_{B_{1g}}(\omega)$  [1] has been dropped as the real part of the electronic response  $\chi'_{B_{1g}}(\omega)$  in the normal state turns out to be a smooth function of  $\omega$  close to  $\omega_{B_{1g}}$ . Using these expressions we obtain the resonance frequency of the phonon  $\hat{\omega}_{B_{1g}}$

$$\hat{\omega}_{B_{1g}}^2 = \omega_{B_{1g}}^2 [1 - \lambda(\omega_{B_{1g}})] \quad (16)$$

which depends only on the electron-phonon coupling. The position of the antiresonance  $\omega_a^2$  can be given as

$$\omega_a^2 = \omega_{B_{1g}}^2 [1 + \beta]. \quad (17)$$

Through  $\beta$  the antiresonance frequency depends also on ratio of the photon-phonon coupling  $g_{p-p,B_{1g}}$  to the projected photon-electron coupling  $\gamma_{B_{1g}}$ . The magnitude of these parameters is not important and enters as a multiplicative scale factor determining the absolute cross section in the same way as the density of states  $N_F$ . Finally, electron-phonon coupling leads to a larger line width

$$\Gamma_{B_{1g}}(\omega_{B_{1g}}) = \Gamma_{B_{1g}}^i + g_{B_{1g}}^2 \chi''_{B_{1g}}(\omega_{B_{1g}})/N_F, \quad (18)$$

neglecting strong anisotropy of the electron-electron or electron-impurity self energies.

### III. SAMPLES AND EXPERIMENTAL

The Y-123 crystals were grown in  $\text{BaZrO}_3$  [14] which has been shown to be completely inert and to facilitate the preparation of samples with a purity of better than 99.995%. All crystals were postannealed in pure oxygen and quenched. Temperatures and oxygen partial pressures were adjusted according to the calibration of Lindemer et al. [15]. The resulting oxygen concentrations were approximately 6.0, 6.5, 6.93, and very close to 7.0 for the samples we call antiferromagnetic (AF) insulating, under-doped, optimally doped and over-doped, respectively, in the following. The magnetically determined respective  $T_c$  values and transition widths of the superconducting samples were 53.5 K ( $\Delta T_c = 3$  K), 91.5 ( $\Delta T_c = 0.3$  K), and 87.0 ( $\Delta T_c = 1.0$  K).

The Bi-based samples,  $\text{Bi}_2\text{Sr}_2(\text{Ca}_{1-x}\text{Y}_x)\text{Cu}_2\text{O}_8$  (Bi-2212), were prepared in  $\text{ZrO}$  crucibles. In optimally doped crystals (without Y) the resistively measured  $T_c$  was generally above 91 K with  $\Delta T_c < 2$  K. If  $\text{Ca}^{2+}$  is replaced by  $\text{Y}^{3+}$  (see Fig. 1) holes in the  $\text{CuO}_2$  planes are filled in and  $T_c$  is reduced. At the same time the environment of the planes becomes electrically asymmetric. The samples we used contained 38% Y and 100% Y, respectively. The superconducting sample (38%) was well in the underdoped range of the phase diagram with a  $T_c$  of 57 K ( $\Delta T_c = 5$  K). Bi-2212 is not stable at the stoichiometric composition and there is always excess Bi in the crystals (typically  $\text{Bi}_{2.1}$  instead of  $\text{Bi}_2$ ) [16,17] which is found predominantly in the Ca (Y) position. In addition, a small amount of Sr may be replaced by Ca or Y. Therefore, the environment of the Cu-O plane is by far less ordered than Y-123. In general, it cannot be expected for Bi-2212 that a crystal quality comparable to the one of Y-123 is obtainable. By partially substituting Bi with Pb the modulation along the crystallographic b-axis can be changed or even suppressed completely [19]. In the sample we used the Laue pattern still showed an indication of a twofold symmetry but it is reasonable to assume that the distortion is smaller than in Pb-free samples.

The experiments were performed in back-scattering geometry using a double monochromator with single-channel detection and the resolution set at  $8 \text{ cm}^{-1}$ . This is sufficient as the total widths of the narrowest lines are roughly twice as large and add quadratically to the resolution. For excitation the  $\text{Ar}^+$  line at 476 nm was selected. The maximal power was 4 mW in order to keep the laser-induced heating below 15 K. The beam was focused to a spot of approximately  $50 \times 150 \mu\text{m}^2$ . For the study of the excitations we were interested in the polarizations of the incoming and outgoing photons were always parallel to the planes. The coordinate system is locked to the Cu-O bonds with  $x = [100]$ ,  $x' = [110]$ , etc. All symmetries refer to a tetragonal pointgroup.  $B_{1g}$  phonon and continuum are projected out with  $x'y'$  polarization.

### IV. RESULTS

Results for Y-123 obtained at  $B_{1g}$  symmetry ( $x'y'$ ) are plotted in Fig. 3. All spectra are divided by the Bose-Einstein thermal function in order to get the response  $\text{Im}\chi$  as given in Eq. (12). As a result of doping the shape of the  $B_{1g}$  phonon at approximately  $330 \text{ cm}^{-1}$  changes considerably. For the AF and slightly doped sample it is narrow and close to a Lorentzian. When carriers are added the line broadens and becomes more asymmetric exhibiting a Fano-type dependence on frequency. The oscillator strength of the phonon decreases while the  $B_{1g}$  continuum gains intensity [20]. As a consequence the intensity ratio  $I_{\text{phonon}}$  to  $I_{\text{continuum}}$  decreases by a factor of at least 20. We emphasize that the low energy continuum vanishes almost completely in the AF crystal, hence supporting the interpretation in terms of charge excitations.

In optimally doped Bi-2212 (Fig. 4 (c)) the  $B_{1g}$  phonon line is much weaker while the continuum has roughly the same cross section as comparable Y-123 (Fig. 3 (c)). The bigger line width comes at least in part from inhomogeneous

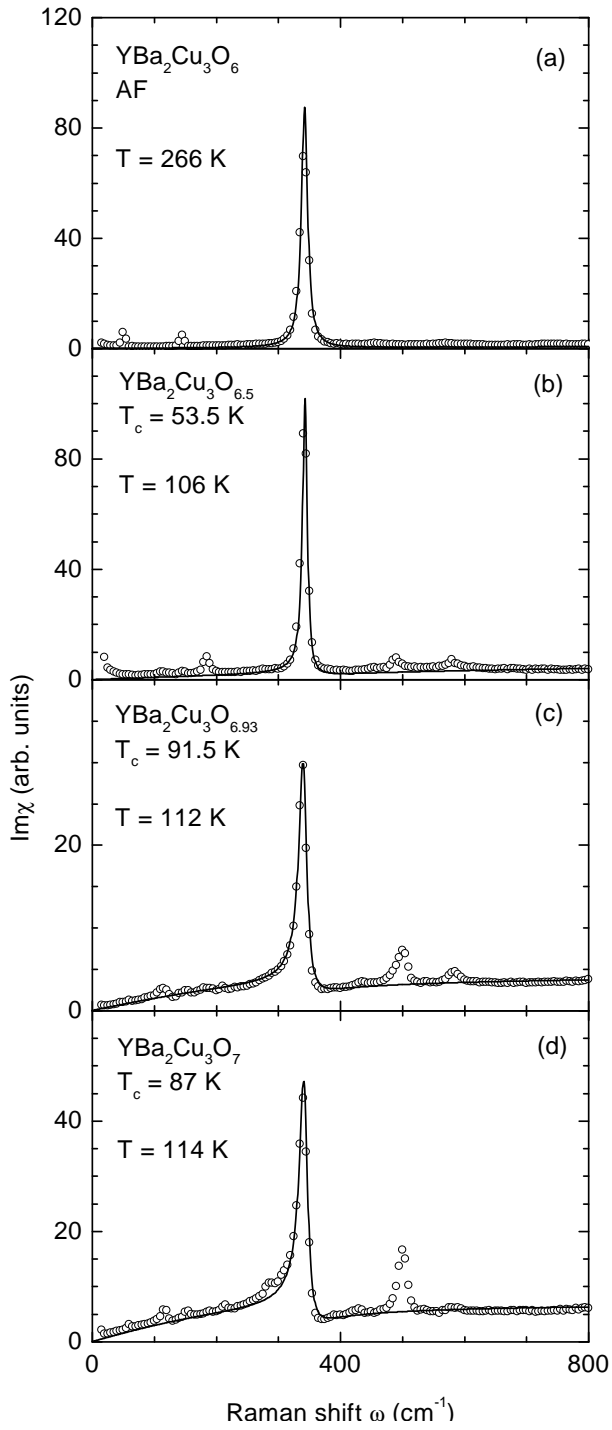


FIG. 3.  $B_{1g}$  spectra for differently doped  $\text{YBa}_2\text{Cu}_3\text{O}_{6+x}$  as indicated. Shown are experimental data (after division by the Bose factor) and theoretical results from the crystal field model (Eqs. (12)–(18)). The parameters used are defined in the text and compiled in Table I.

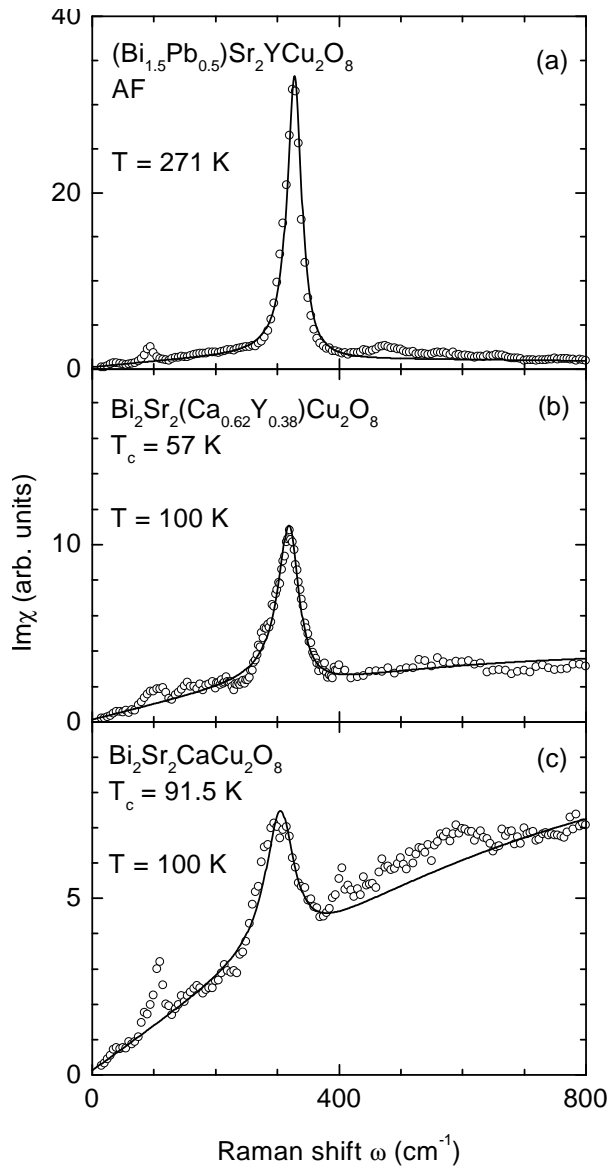


FIG. 4.  $B_{1g}$  spectra for differently doped  $(\text{Bi},\text{Pb})\text{Sr}_2(\text{Ca},\text{Y})\text{Cu}_2\text{O}_8$  as indicated. Shown are experimental data (after division by the Bose factor) and theoretical results from the crystal field model (Eqs. (12)–(18)). The parameters used are defined in the text and compiled in Table I.

Fig.	Sample	$T_c$ [K]	Scale	$\alpha$	$\tau_{B_{1g}}^* \text{ }^{-1}$ [cm $^{-1}$ ]	$\Gamma_{B_{1g}}^i$ [cm $^{-1}$ ]	$\omega_{B_{1g}}$ [cm $^{-1}$ ]	$\omega_a$ [cm $^{-1}$ ]	$\lambda$	$\hat{\omega}_{B_{1g}}$ [cm $^{-1}$ ]	$T$ [K]	$\beta'$	$\omega_c$ [cm $^{-1}$ ]
3(a)	YBa <sub>2</sub> Cu <sub>3</sub> O <sub>6</sub>	AF	4	0.55	3000	6.0	342	345.5	0.000585	342.1	266	3.3	12000
3(b)	YBa <sub>2</sub> Cu <sub>3</sub> O <sub>6.5</sub>	53.5	22	0.55	3000	4.0	347.5	352.5	0.0257	343	106	3.3	12000
3(c)	YBa <sub>2</sub> Cu <sub>3</sub> O <sub>6.93</sub>	91.5	20	0.95	1200	6.5	348	349.3	0.0426	340.5	112	3.3	12000
3(d)	YBa <sub>2</sub> Cu <sub>3</sub> O <sub>7</sub>	87.0	30	0.75	900	6.0	352	352.5	0.056	342	114	3.3	12000
4(a)	(Bi <sub>1.5</sub> Pb <sub>0.5</sub> )Sr <sub>2</sub> YCu <sub>2</sub> O <sub>8</sub>	AF	2.4	0	400	14	328.5	336.2	0.00213	328.15	271	3.3	12000
4(b)	Bi <sub>2</sub> Sr <sub>2</sub> Y <sub>0.38</sub> Ca <sub>0.62</sub> Cu <sub>2</sub> O <sub>8</sub>	57.0	10	0.2	1200	20	322	326	0.0124	320	100	3.3	12000
4(c)	Bi <sub>2</sub> Sr <sub>2</sub> CaCu <sub>2</sub> O <sub>8</sub>	91.5	20	0.1	1600	28	305.2	306.05	0.00131	305	100	3.3	12000

TABLE I. Summary of fitting parameters used in Figs. 3 and 4.  $T_c$  is the superconducting critical temperature,  $T$  the measuring temperature. AF indicates that the sample is antiferromagnetic and insulating. The seven parameters in the third column are the fitted parameters. The actual Fano profile determines the parameters  $\omega_{B_{1g}}$ ,  $\omega_a$ , and  $\lambda$  which depend only weakly on  $\alpha$ ,  $\tau_{B_{1g}}^* \text{ }^{-1}$ ,  $\beta'$ , and  $\omega_c$  (see text).  $\hat{\omega}_{B_{1g}}$  is calculated from  $\omega_{B_{1g}}$  and  $\lambda$ . The last column are fixed parameters. A scale factor was multiplied to Eq. (12) to account for the overall magnitude of the cross section. The scale factor is proportional to the density of states at the Fermi energy  $N_F$  and is, as expected, very small in the AF samples.

broadening as explained above which manifests itself in the large intrinsic line width (see Table I). If Y is doped in for Ca a new line at approximately 315 cm $^{-1}$  starts to gain intensity very rapidly (Fig. 4 (a) and (b)). A reminder of the line found in Y-free crystals is still seen as a shoulder on the left-hand side of the new one (Fig. 4 (b)). This tells us that the Y is not completely homogeneously distributed in the underdoped sample. Most likely, the Y replaces big regions of the Ca planes, just like in Y-123 where upon oxygen doping clusters of longer and shorter fractions the chains build up depending on the conditions of preparation [18]. So, in addition to changing the charge balance around the CuO<sub>2</sub> plane, defects are introduced in its vicinity which are seen in both the phononic and the electronic properties. Apparently the intrinsic linewidth in the AF sample is somewhat smaller than in the metallic ones. This comes most likely from the additional doping with Pb which is used to suppress the superstructure of the BiO<sub>2</sub> layers and the related orthorhombic distortion of the unit cell. The integrated cross section is now as large as in AF Y-123 [compare Fig. 3 (a) and Fig. 4 (a)]. This is further independent evidence for the model proposed.

## V. DISCUSSION AND CONNECTION TO BUCKLING

Excellent fits to the data on optimally-doped YBa<sub>2</sub>Cu<sub>3</sub>O<sub>7- $\delta$</sub>  in both the superconducting and normal states were given in [1], which when interpreted supported evidence for  $d_{x^2-y^2}$ -pairing in this material. We have extended these results by examining normal state data of different samples and dopings. We note that a completely new set of Y-123 single crystals with superior quality (see section III) is used here.

We find that once again very good fits to the data can be obtained on four and three differently doped samples of Y-123 and Bi-2212, respectively. For all fits given in Figs. 3 and 4, the values used to calculate the susceptibilities of nested Fermi liquid theory and the phonon lineshapes are summarized in Table I.

Eight parameters ( $\alpha$ ,  $\tau_{B_{1g}}^*$ ,  $\Gamma_{B_{1g}}^i$ ,  $\omega_{B_{1g}}$ ,  $\omega_a$ ,  $\lambda$ ,  $\hat{\omega}_{B_{1g}}$ , and an overall scale factor) are used to provide the fits in Figs. 3 and 4. However, we do not have eight separate degrees of freedom.  $\alpha$ ,  $\tau_{B_{1g}}^*$ , and the overall scale factor are chosen to reproduce the continuum for frequencies away from the phonon.  $\tau_{B_{1g}}^*$  determines the low frequency part of the continuum while  $\alpha$  determines the high frequency part. The uncertainty in these parameters is less than 10%. In addition, the parameters  $\alpha$  and  $\beta'$  are in the narrow range imposed by the nFL model. [3] Then  $\hat{\omega}_{B_{1g}}$  is chosen to locate the center of the phonon line, which can be accurately placed to within a fraction of a wavenumber (i.e. much better than the experimental resolution). Next  $\lambda$  is chosen to reproduce the local asymmetry around the phonon line (Fano). This automatically fixes  $\omega_{B_{1g}}$  via Eq. (16) and sets the damping from the coupled electron-phonon system. Then, the intrinsic line width  $\Gamma_{B_{1g}}^i$  is set to account for any remaining damping needed to account for the phonon linewidth. An indication of the stability is the almost constant intrinsic line width in Y-123. Indeed these samples are comparable and the unit cell changes only slightly. On the other hand, it is not surprising that the intrinsic line width is not constant in Bi-2212 since the environment of the planes and even the total crystallographic structure changes

considerably on doping. Finally,  $\omega_a$  is then chosen to set the overall intensity of the phonon relative to the electronic continuum and to pinpoint the minimum of the spectrum on the high frequency side of the phonon. In summary, each parameter is independently chosen and the accuracy of the fit can be determined by the agreement of the theory to the experimental background and the phonon's position, intensity, asymmetry, linewidth, and local high frequency minimum. Therefore we are confident that the parameters used are accurate to within the 10% level. Should further constraints be imposed (i.e. by a more accurate theory for the continuum or the phonon-photon coupling constant), it would be straightforward to adapt the theory accordingly.

We now can make a comparison to the crystal field model predictions for the electron-phonon coupling constant. We see from the fits that for the Y-123 compounds the electron-phonon coupling increases up to a factor of two with increasing doping. This can be understood in part by an increase in the density of states at the Fermi level with increased oxygen doping as the van Hove contribution moves closer to the Fermi level (see Fig. 2). Our calculations using Eq. (14) yield the following values for  $\lambda$  as a function of doping: for  $\lambda = 0.0321$  for  $\langle n \rangle = 0.875$  (underdoped, Fig. 3b),  $\lambda = 0.0382$  for  $\langle n \rangle = 0.85$  (optimally doped, Fig. 3c), and  $\lambda = 0.0482$  for  $\langle n \rangle = 0.8$  (overdoped, Fig. 3d). Here we have taken  $T = 100K$ ,  $\omega_{B_{1g}} = 348\text{cm}^{-1}$ ,  $M = 16m_P$ , where  $m_P$  is the proton mass, and used a value of the electric field which is  $1.3\text{V}/\text{\AA}$  [23]. We observe that these values of  $\lambda$  are quite close to the values used to obtain the fits in Figs. 3 (b)–(d). Given the values of  $t'/t$ ,  $t$ , and  $\varepsilon$  are taken to be independent of doping, the agreement is quite good. The agreement could be refined once parameter choices for various levels of doping are determined via, e.g., fitting to experimentally observed Fermi surfaces.

We can connect the value of the electric field used to account for the observed buckling of the  $\text{CuO}_2$  plane in Y-123. The electric field  $E$  perpendicular to the  $\text{CuO}_2$  plane results in an  $A_{1g}$ -type static distortion of the plane since the charges of oxygen and copper are different. It is very hard to perform a complete calculation as the electric field is different at the Cu and the O sites. Furthermore all the lattice forces have to be known. For an estimation of the buckling, however, a simplified model is sufficient [12] where Cu is pinned rigidly to the elementary cell and the oxygen moves in a harmonic potential being characterized by the frequency of the  $A_{1g}$  phonon at  $\omega_{A_{1g}} = 435\text{ cm}^{-1}$  [21]. The restoring force at the buckling amplitude  $\Delta z$  must balance the electric force acting on the oxygen with charge  $q = -1.75e$ . Thus,  $qE = M\omega_{A_{1g}}^2 \Delta z$  must hold. With the experimental value  $\Delta z = 0.24\text{\AA}$  [12],  $E = 1.53\text{V}/\text{\AA}$  is obtained which is close both to the  $1.3\text{V}/\text{\AA}$  used for estimating the electron-phonon coupling strength and to the theoretically calculated number [23]. On the other hand, in the case of  $\text{CuO}_2$  planes in a more symmetrical environment as in Bi-2212 and the infinite-layer compound  $\text{CaCuO}_2$  the buckling, if it exists at all, is at least an order of magnitude smaller as found in structural studies [24,25].

At the same time, the electron-phonon coupling for optimally doped Bi-2212 (Fig. 4c) obtained from the fit is more than one order of magnitude smaller than for any of the metallic Y-123 compounds and, as a result, the weight of the phonon is also reduced by at least the same amount. Indeed, in our model we would expect that the electron-phonon coupling is significantly smaller since the crystal electric field must be much weaker in this compound than in Y-123 (see Fig. 1). We attribute then the small electron-phonon coupling to a much smaller local asymmetry. A weaker spontaneous symmetry breaking is also possible.

To test this idea we presented measurements of a sample of Bi-2212 which has been doped with small amounts of Y in place of Ca (Fig. 4b). Since here the valence of Y (+3) is different from that of Ca (+2), once again the mirror plane symmetry is broken and we would expect a much larger electron-phonon coupling than in the undoped compound. The fit to the  $B_{1g}$  data using Eq. (12) is given in Fig. 4(b) and yields  $\lambda = 0.0124$ . The coupling constant is indeed increased over that of the optimally doped compound by an order of magnitude when Y is introduced and in accordance the intensity of the phonon line is also essentially enhanced. This trend continues in the AF sample Fig. 4(a), and the phonon cross section is now similar to that in Y-123.

The intensity of the continuum in Bi-2212:Y does not approach zero as one would expect for an insulator. In-Y-123, too, the continuum is not vanish identically but is significantly smaller. At present, we do not know the origin of this intensity. It can be either photoexcited carriers as observed in semiconductors [22], an effect of remaining carriers, or coupling of the phonon to the spin system [26]. As a consequence the coupling  $\lambda$  is not as small, though reduced considerably, as to be expected and actually observed in Y-123. This again gives strong support for the crystal field coupling model as the driving source of electron-phonon coupling.

## VI. SUMMARY AND CONCLUSIONS

In summary, studying Y-123 with different doping levels we have shown that the breaking of the local reflection symmetry through the  $\text{CuO}_2$  planes due to the position and charges of the neighboring atoms results in an electric field across the planes which is sufficiently strong to produce both the observed buckling and the strong electron-phonon coupling being responsible for the Fano-type line shape of the respective  $B_{1g}$  mode. In order to check this

idea experiments were performed on Bi-2212 with and without Y doping. While the sample without Y shows very weak electron-phonon coupling, the interaction is enhanced by an order of magnitude and becomes comparable to the one in Y-123 if the local reflection symmetry is broken by replacing part of the Ca by Y. (For Bi-2212 and  $\text{CaCuO}_2$  there is no experimental indication for spontaneous symmetry breaking.) As doping Bi-2212 by Y results in a change of  $T_c$  from  $T_c = 91.5\text{K}$  to  $T_c = 57\text{K}$  accompanied by a large increase of the coupling  $\lambda$ , the  $\omega = 330\text{cm}^{-1}$  phonon can not play an important role for the superconductivity, in agreement with the conclusion of Savrasov and Andersen [27]. We conclude that the symmetry breaking due to the composition can explain both the buckling of the planes and the strong linear electron-phonon coupling in the two types of material. One should keep in mind that spontaneous symmetry breaking can occur also in other materials like  $\text{La}_{2-x}\text{Sr}_x\text{CuO}_4$  and determine the properties. Further experimental and theoretical studies of  $\text{CaCuO}_2$  would be useful. It is of interest in the present context that the so called infinite layer material  $\text{CaCuO}_2$  does not show any sign of buckling [24], consistently with the symmetric position of the  $\text{CuO}_2$  plane.

## ACKNOWLEDGMENTS

We gratefully acknowledge enlightening discussions with W. Pickett, O.K. Andersen, and B. Györfy. This work was supported by the Hungarian National Research Fund under Grant Nos. OTKA T020030, T016740, T02228/1996, T024005/1997. Acknowledgment (T.P.D.) is made to the Donors of The Petroleum Research Fund, administered by the American Chemical Society, for partial support of this research. A. Z. is grateful for the support by the Humboldt Foundation. The experiments have been supported partially by the Bayerische Forschungsstiftung through the “Forschungsverbund Hochtemperatur- Supraleiter (FORSUPRA)” We are grateful to the BMBF for financial support via the program “Bilaterale Wissenschaftlich-Technische Zusammenarbeit” under grant no. WTZ-UNG-052-96. One of us (T.P.D.) was partially supported by the American Hungarian Joint Fund No. 587.

---

- [1] T. P. Devereaux, A. Virosztek and A. Zawadowski, Phys. Rev. B **51**, 505 (1995).
- [2] T.P. Devereaux, A. Virosztek and A. Zawadowski, M. Opel, P.F. Müller, C. Hoffman, R. Philipp, R. Nemetschek, R. Hackl, H. Berger, L. Forró, A. Erb, and E. Walker, Solid State Commun. **108**, 407 (1998).
- [3] A. Virosztek and J. Ruvalds, Phys. Rev. B **45**, 347 (1992).
- [4] A. Zawadowski and M. Cardona, Phys. Rev. B **42**, 10732 (1990).
- [5] T. P. Devereaux and A. P. Kampf, cond-mat/9711039.
- [6] E. Sherman, R. Li, and R. Feile, Solid State Commun. **94**, 851 (1995) and Phys. Rev. B **52**, R15757 (1995).
- [7] S. Sugai and M. Sato, Phys. Rev. B **40**, 9292 (1989); M. Boekholt *et al.*, Physica C **185-189**, 1035 (1991); D. H. Leach *et al.*, Sol. State Commun. **88**, 457 (1993); M. Kakihana *et al.*, Phys. Rev B **53**, 11796 (1996).
- [8] S.L. Cooper *et al.* Phys. Ref. B **37**, 5920 (1988); B. Friedl, C. Thomsen, and M. Cardona, Phys. Rev. Lett. **65**, 915 (1990); R. Li *et al.*, Physica C **175**, 89 (1991); D. Reznik *et al.*, Phys. Rev. B **48**, 7624 (1993); X. K. Chen *et al.*, *ibid.* **48**, 10530 (1993).
- [9] E. Altendorf *et al.*, Phys. Rev. B **47**, 8140 (1993).
- [10] R. Zeyher and G. Zwicknagl, Z. Phys. B **78**, 175 (1990); F. Marsiglio, Phys. Rev. B **47**, 5419 (1993); M. E. Flatté, Phys. Rev. Lett. **70**, 658 (1993); C. Jiang and C. Carbotte, Phys. Rev B **50**, 9449 (1994); T. P. Devereaux, *ibid.*, 10287 (1994). A. Bill, V. Hizhnyakov, and E. Sigmund, *ibid.*, 7637 (1995).
- [11] O. K. Andersen *et.al.*, J. Low Temp. Phys. **105**, 285 (1996).
- [12] J. D. Jorgensen *et.al.*, Phys. Rev. B **36**, 3608 (1987).
- [13] We note that the definitions of  $g$  and  $\lambda$  given in Equations (13-14) are different than those used in Ref. [1]. This is simply because in this paper we do not take a flat density of states.
- [14] A. Erb, E. Walker, J.-Y. Genoud, and R. Flükiger, Physica C **282- 287**, 89 (1997).
- [15] T. B. Lindemer, J. F. Hunley, J. E. Gates, A. L. Sutton, J. Brynestad; C. R. Hubbard, and P. K. Gallagher, J. Am. Ceram. Soc. **71**, 1775 (1992).
- [16] R. E. Gladyshevskii and R. Flükiger, Acta Cryst. B **52**, 38 (1996).
- [17] B. Revaz, private communication.
- [18] G. Oszlányi *et.al.*, Physica C **167**, 157 (1990); S. Pekker *et.al.*, Physica C **181**, 11 (1991); A. Erb, J.-Y. Genoud, F. Marti, M. Daumling, E. Walker, and R. Flükiger, J. Low. Temp. Phys. **105**, 1023 (1996).
- [19] H. Berger, private communication.

- [20] T. Katsufuji, Y. Tokura, T. Ido, and S. Uchida, Phys. Rev. B **48**, 16131 (1993); X. K. Chen, J. G. Naeini, K. C. Hewitt, J. C. Irwin, R. Liang, and W. N. Hardy, Phys. Rev. B **56**, R513 (1997); R. Nemetschek, M. Opel, C. Hoffmann, P. F. Müller, R. Hackl, H. Berger, L. Forró, A. Erb, and E. Walker, Phys. Rev. Lett. **78**, 4837 (1997).
- [21] This assumption is a reasonable approximation for results obtained by ab-initio frozen-phonon calculations, [C.O. Rodriguez *et al.* Phys. Rev. B **42**, 2692 (1990)].
- [22] G. Abstreiter, M. Cardona, and A. Pinczuk, Topics in Applied Physics **54**, 5 (Springer-Verlag, Berlin, 1984).
- [23] J. Li and J. Ladik, Sol. State Commun. **95**, 35 (1995).
- [24] J. Karpinski *et.al.*, Physica C **234**, 10 (1994).
- [25] It remains to study why the electronic energy calculations provide a spontaneous symmetry breaking for CaCuO<sub>2</sub>.
- [26] B. Normand *et al*, Phys. Rev. B **53**, 856 (1996);
- [27] S. Y. Savrasov and O. K. Andersen, Phys. Rev. Lett. **77**, 4430 (1996).